Effect of Higher Modes on Waveguide Aperture Covered by a Dielectric Slab in the Liquid

[#]Nozomu Ishii [1,2], Yukihiro Miyota [3], Lira Hamada[2], Soichi Watanabe [2]
[1] Faculty of Engineering, Niigata University
8050, Ikarashi 2-nocho, Nishi-ku, Niigata, 950-2181 Japan, nishii@eng.niigata-u.ac.jp
[2] National Institute of Information and Communications Technology
4-2-1, Nukui-Kitamachi, Koganei, Tokyo, 184-8795 Japan
[3] NTT Advanced Technology
3-9-11, Midori-cho, Musashino, Tokyo, 182-0012 Japan

Abstract

A novel calibration method for a probe used in a standard SAR measurement system is examined. In our experimental model, the E-field distribution is generated by the waveguide aperture covered with a dielectric slab. Simulated and measured E-field distributions suggest that the distribution consist of not only TE_{10} mode but also higher modes, for example, TM_{12} mode.

Keywords : SAR, Probe Calibration, Liquid, Waveguide Aperture, Dielectric Slab, Higher Mode

1. Introduction

SAR (Specific Absorption Rate) of mobile communication devices is generally measured by inserting an electrical field probe in tissue-equivalent liquid surrounded by a shell shaped like the geometry of a human body. The probe has to be calibrated by relating its output voltage to the electrical field intensity at its position in the liquid. One of the calibration methods for the probe uses the tank for the tissue-equivalent liquid surrounded by the side walls of the rectangular waveguide and a dielectric spacer as the bottom wall [1]. This method is generally used for the SAR probe calibration, however, has a drawback that the effect of the diameter of the probe cannot be ignored as the frequency is higher because of smaller cross-sectional dimension of the waveguide. To overcome the difficulty, the authors have proposed an alternative calibration method for the probe [2]. In our proposed method, the side walls of the tank in the standard method are removed, however, the transition function from an air-filled waveguide to the liquid via the dielectric spacer can be preserved. In both methods, the electric field distribution extremely near the aperture is approximately given by $\boldsymbol{e}(x,y)e^{-\gamma z}$, where $\boldsymbol{e}(x,y)$ is transverse electric field distribution at the waveguide aperture and γ is propagation constant of the tissue-equivalent liquid.

Experimentally to validate our proposed calibration method, we have constructed the waveguide aperture covered by the dielectric slab in the tissue-equivalent liquid at 5.2GHz, as shown in Fig. 1. The difference between theoretical and experimental models is that the former has no flange so that the dielectric slab is inserted into the waveguide tube as shown in Fig. 2, while the latter has a finite flange so that the waveguide aperture and the flange are covered with the dielectric slab as shown in Fig. 1, where the transverse distribution at the surface of the slab is different from that due to the dominant mode of the waveguide. In this paper, this difference is numerically examined and analyzed by decomposing the numerical E-field distribution into waveguide's modes.

2. Approximation of Field Distribution Radiated by Waveguide Aperture

Fig. 2 shows a theoretical model of our proposed calibration method. The rectangular waveguide aperture is immersed in the phantom liquid and is separated by a dielectric slab. If the transverse electric field distribution on the aperture is given by TE_{mn}/TM_{mn} modes of the waveguide,

$$\boldsymbol{e}_{mn}(x,y) = \hat{\boldsymbol{y}} \sin a_m\left(x+\frac{a}{2}\right)\cos b_n\left(y+\frac{b}{2}\right), \tag{1}$$

then the electrical field distribution along the z axis is approximately given as

$$\boldsymbol{E}_{mn}(x,y,z) \approx \hat{\boldsymbol{y}} \sin a_m\left(x+\frac{a}{2}\right)\cos b_n\left(y+\frac{b}{2}\right)\exp\left\{-\left(\gamma+\frac{a_m^2+b_n^2}{2\gamma}\right)z\right\}$$

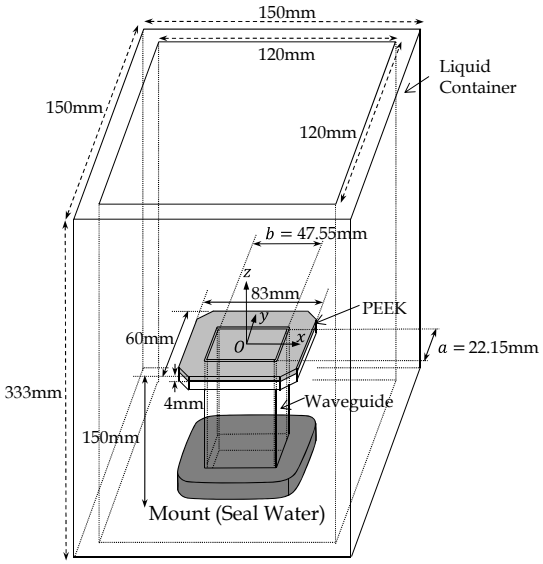

Figure 1: A waveguide aperture in the container filled with the tissue-equivalent liquid at 5.2GHz.

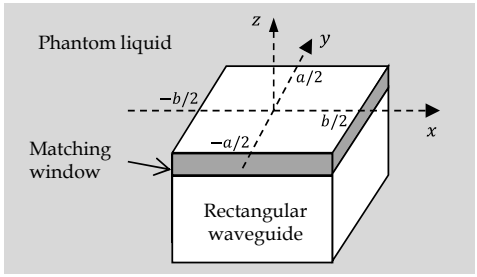

Figure 2: A waveguide aperture immersed in the liquid used as a theoretical model.

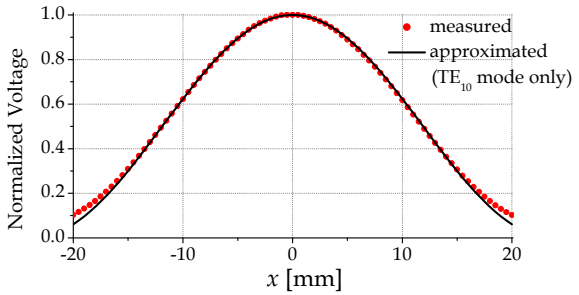

Figure 3: Normalized voltage of the probe along the x axis.

$$\approx \hat{\boldsymbol{y}} \sin a_m\left(x+\frac{a}{2}\right)\cos b_n\left(y+\frac{b}{2}\right)e^{-\gamma z}\,, \tag{2}$$

where $a_m = m\pi/a$, $b_n = n\pi/b$ and we assumed that $a_m^2 + b_n^2 \ll 2|\gamma^2|$ for the tissue-equivalent liquid. In the derivation of equation (2), we use the paraxial approximation and an approximate formula for the complex error function, $\mathrm{erf}(w) \approx 1 - e^{-w^2}/\sqrt{\pi}w$ for $|w| \ll 1$ [2]. As expected, the E-field distribution of the TE_{10} mode for our proposed calibration method is equal to that for the standard calibration method. This means that the procedure of the standard calibration method can also be used for our proposed calibration method.

3. Measured and Simulated Field Distribution Over Waveguide Aperture

The electric field distribution can be measured by using a standard probe calibration system. The output voltage of the probe, V, is proportional to the square of the electric field intensity at the probe's location, E^2, so that the calibration factor can be given as $\mathrm{CF} = V/E^2$. Fig. 3 shows the distribution of the electric field intensity along the x axis on the plane of $z = 5\mathrm{mm}$ in the liquid region, at 5.2GHz. The measured range of y is limited to $|y| \leq -20\mathrm{mm}$. Input power into the waveguide is 22.0dBm and the dielectric slab (PEEK) can be assumed to be lossless and has a thickness of 4mm and a relative dielectric constant of 3.4. The probe and detector used are SPEAG EX3DV4 and DAE4, respectively. Measured relative dielectric constant and conductivity of the liquid (NTT-AT HT5200) at 5.2GHz are 35.58 and 4.49S/m, respectively. For $|y| \leq 12\mathrm{mm}$, the relative errors between detected voltage and approximated voltage which is estimated based on TE_{10} mode contribution are within 1% so that the electric field intensity obeys the TE_{10} mode, i.e., $\cos(\pi x/a)$ near the center of the waveguide aperture.

Fig. 4 shows the transverse electric field distribution on the plane of $z = 5\mathrm{mm}$, in the range of $|x| \leq 10\mathrm{mm}$ and $|y| \leq 10\mathrm{mm}$. When initial position of the probe was shifted off the center of the waveguide, we could not observe the distribution due to only TE_{10} mode. Therefore, the field distribution consists of not only dominant mode but also higher modes of the waveguide. Rigorously, the problem cannot be decomposed into completely discrete waveguide modes, that is, it should be treated by using hybrid of mode expansion and spectral representation [3]. However, to facilitate our intuition of the problem, we simply discuss the electromagnetic behavior from the

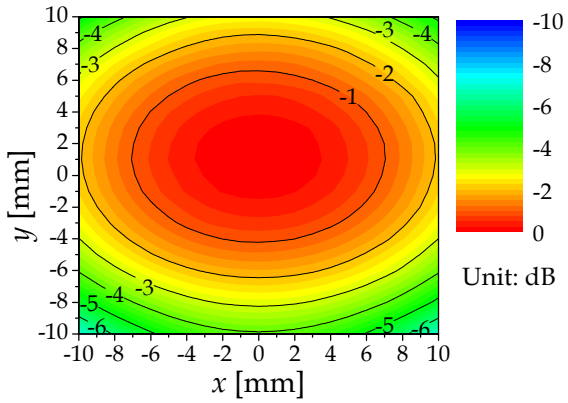

Figure 4: Normalized E-field distribution at $z = 5\text{mm}$ measured by the probe system.

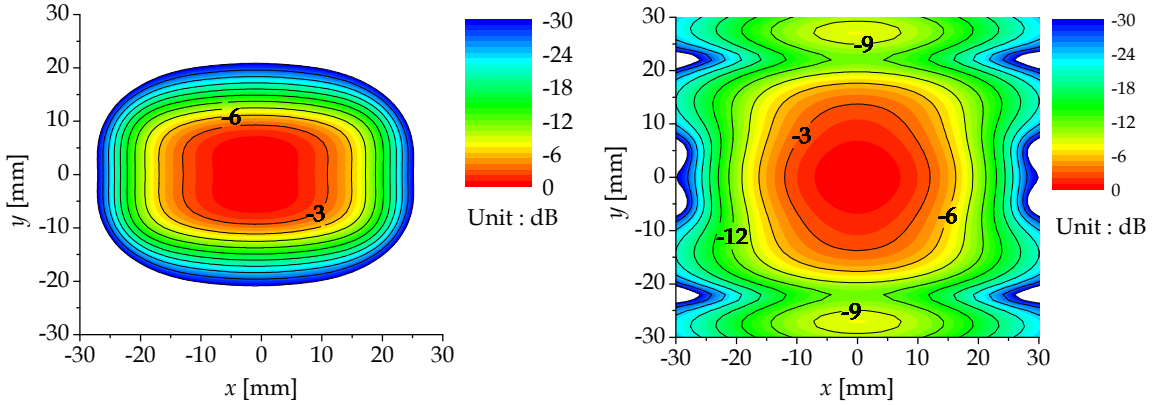

(a) Theoretical Model (b) Experimental Model

Figure 5: Normalized E-field distribution at $z = 5\text{mm}$ calculated by SEMCAD (FDTD simulator).

viewpoint of the mode analysis in the rest of the paper. Fig. 5 shows the transverse electric field distribution on the plane of $z = 5\text{mm}$ for theoretical and experimental models, calculated by FDTD simulator. We can see that two distributions are not identical. For the theoretical model, the distribution is the same as the TE_{10} mode of the waveguide except the neighborhood of the waveguide walls. However, for the experimental model, the distribution is different from the TE_{10} mode. This fact suggests that the latter should consist of the dominant mode and some higher modes.

4. Mode Analysis

4.1 Outline of Mode Analysis

To examine what modes largely contribute to forming the distribution, we introduce the mode analysis. We assume that the transverse electric field distribution at the surface of the dielectric slab, $\boldsymbol{E}(x, y, 0)$, can be expanded by the modal vector function, $\boldsymbol{e}_l(x, y)$, for mode $\#l$, as

$$\boldsymbol{E}(x, y, 0) = \sum_l c_l \boldsymbol{e}_l(x, y)\,. \tag{3}$$

By using the feature of the normalization and orthogonality of the modal vector function, the excitation coefficient, c_l, can be given as

$$c_l = \int_{-a/2}^{a/2} \int_{-b/2}^{b/2} \boldsymbol{E}(x, y, 0) \cdot \boldsymbol{e}_l(x, y) dy dx. \tag{4}$$

When the distribution is given by the simulator, we should approximate the above integral by double summations as

$$c_l \approx \sum_{i=1}^{N_x} \sum_{j=1}^{N_y} \boldsymbol{E}(x_i, y_j, 0) \cdot \boldsymbol{e}_l(x_i, y_j) \Delta x_i \Delta y_j. \tag{5}$$

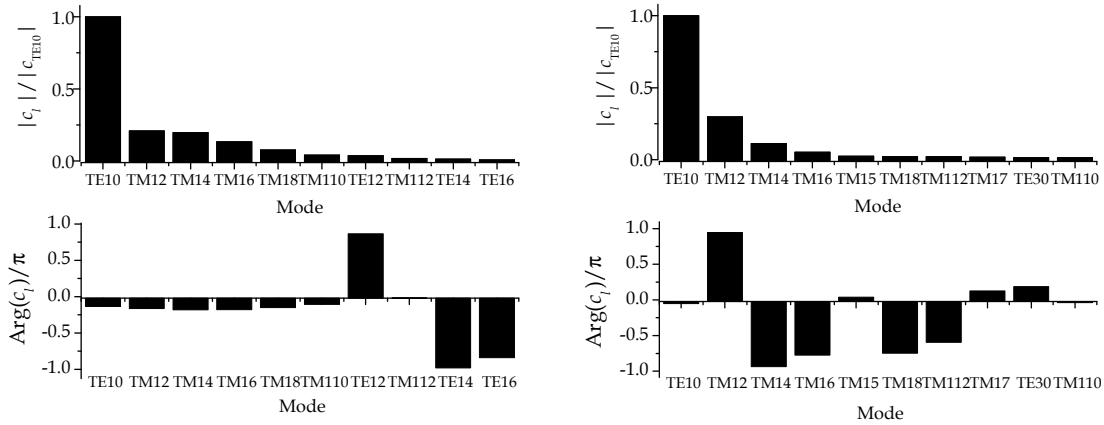

(a) Theoretical Model (b) Experimental Model

Figure 6: Mode decomposition of electric field distribution at $z = 0$mm calculated by SEMCAD.

The simulated distribution is sampled at the points of (x_i, y_j). Δx_i and Δy_i are the distances between adjacent sampling points and N_x and N_y are numbers of sampling points in the x and y directions.

4.2 Results of Mode Analysis

Fig. 6 shows the magnitude of the excitation coefficients for the top five modes when the air-filled waveguide is driven by the TE_{10} mode. For symmetry, TE_{mn}/TM_{mn} modes where m is odd and n is even would be excited. As shown in Fig. 6, TE_{10} mode is most excited and also TM_{12} and TM_{14} modes are not ignored to form the distribution in both the theoretical and experimental models. However, the excitation coefficients TE_{10} and TM_{12} modes are in phase for the theoretical model and out of phase for the experimental model so that the distribution for the experimental model are different from the TE_{10} mode. In addition, it is known that a similar configuration where an infinite liquid is replaced by a grounded planar dielectric slab can support the occurrence of TM_{12} mode [4].

5. Conclusions

An alternative method for calibrating the probe used in the standard SAR measurement system is examined. If the distribution of the electric field at the interface between the dielectric slab and liquid is given by TE_{mn}/TM_{mn} modes of the waveguide, we can find an approximate and closed form for the distribution in the extremely near-field region by means of the paraxial approximation and complex error function. For the experimental model, the distribution is different from the dominant TE_{10} mode, because of the existence of the higher modes, for example, TM_{12} mode. This fact was found from the FDTD simulation and modal expansion technique. In future, we are going to examine the reason why the slight difference between theoretical and experimental models in the attenuation curve can be observed by the FDTD simulation. Also, the rigorous hybrid analysis of modal expansion and spectral representation should be introduced to improve our model.

References

[1] IEC, International Standard 62209-1, Feb. 2005.

[2] N. Ishii et al., “Field distribution by open waveguide in the tissue-equivalent liquid,” Proc. 2010 Asia-Pacific Radio Science Conference, Toyama, Japan, KAE-4, 2010.

[3] K. J. Bois et al., “Multimode solution for the reflection properties of an open-ended rectangular waveguide radiating into a dielectric half-space: the forward and inverse problems,” IEEE Trans. Inst. & Meas., Vol. 48, No. 6, pp.1131-1140, Dec. 1999.

[4] H. Hirano et al., “Field analysis in a lossy dielectric sandwiched between a flanged rectangular waveguide and conducting plane,” Electron. Comm. Japan Pt 2: Electron., Vol. 83, pp.52-64, 2000.

Acknowledgments

This work is partly supported by Grant-in-Aid for Scientific Research from the Japan Society for the Promotion of Science.